JCTC Journal of Chemical Theory and Computation

Article

Cite This: J. Chem. Theory Comput. 2017, 13, 5217-5230

pubs.acs.org/JCTC

A Computational Scheme To Evaluate Hamaker Constants of Molecules with Practical Size and Anisotropy

Kenta Hongo*,†,‡,§ and Ryo Maezono‖

†Research Center for Advanced Computing Infrastructure, JAIST, Asahidai 1-1, Nomi, Ishikawa 923-1292, Japan

‡Center for Materials Research by Information Integration, Research and Services Division of Materials Data and Integrated System, National Institute for Materials Science, Tsukuba 305-0047, Japan

§PRESTO, Japan Science and Technology Agency (JST), Kawaguchi, Saitama 332-0012, Japan

‖School of Information Science, JAIST, Asahidai 1-1, Nomi, Ishikawa 923-1292, Japan

Supporting Information

ABSTRACT: We propose a computational scheme to evaluate Hamaker constants, A, of molecules with practical sizes and anisotropies. Upon the increasing feasibility of diffusion Monte Carlo (DMC) methods to evaluate binding curves for such molecules to extract the constants, we discussed how to treat the averaging over anisotropy and how to correct the bias due to the nonadditivity. We have developed a computational procedure for dealing with the anisotropy and reducing statistical errors and biases in DMC evaluations, based on possible validations on predicted A. We applied the scheme to cyclohexasilane molecule, Si_6H_{12}, used in "printed electronics" fabrications, getting $A \approx 105 \pm 2$ zJ, being in plausible range supported even by other possible extrapolations. The scheme provided here would open a way to use handy *ab initio* evaluations to predict wettabilities as in the form of materials informatics over broader molecules.

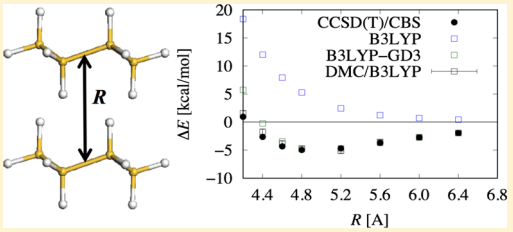

INTRODUCTION

Hamaker constants,[1] A, dominate the wettability[2,3] of solvents, which is one of the critical properties in industrial applications of Sol−Gel methods,[4] including solution processes for semiconductor devices.[5] Microscopic insights on the wettability[2,3] relate the Hamaker constant with molecular interactions, which can be, in principle, evaluated from *ab initio* simulations.[6,7] From the asymptotic behavior of molecular binding curves, or potential energy surfaces (PES), $\sim C_6/R^6$, the Hamaker constant can be computed as $A_{add} = \pi C_6 \rho^2$, provided that only a binding with a single C_6 matters and a naive superposition is expected.[3] The index, "add", then stands for "additive" and ρ denotes the molecular density, which appears when the interactions between each of the infinitesimal fragments are superposed over the volume. Though we can find several such prototypical works[3] of the "*ab initio* assessment" applied to simple and highly symmetric molecules, we would immediately encounter troubles when attempting to apply the framework to practical solute molecules. Most molecules of industrial interest are not so highly symmetric that we cannot generally expect the additivity of the interaction.[8] In these cases, too many alignments of coalescence are possible due to the anisotropy of molecules, bewildering us how to model the coalescence with the confidence for capturing the nature of the system.

The main subject of the present paper is how to estimate A for practical solute molecules via A_{add} with plausible considerations mainly for the anisotropy. Once we could establish such a scheme, such database of molecular interactions aided by recent *ab initio* methods[9] can provide the Hamaker constants over various liquids. It would help to predict, control, and design such solution processes including not only wettabilities but also suspensions and solvabilities by using empirical molecular dynamics simulations.[2]

The present study has been originally motivated by the demand to estimate A for a cyclohexasilane molecule, Si_6H_{12} (CHS), which is used as an ink for "printed electronics" technology to fabricate polycrystalline Si film transistors.[5] The ink including Si-based precursors is sprayed on a substrate, which is sintered to form an amorphous Si thin film, without using expensive vacuum equipment in the conventional semiconductor processes. The ink printing process has hence attracted recent interest for realizing more savings and lower environmental impact technology.[5] Controlling the wettability of these inks is of rather general interest because the technology is about to be applied further to fabricate oxide or carbon nanotube film semiconductor devices[10,11] by using various inks instead of Si-based ones. For going beyond conventional/experimental preparations of inks, several simulations have been made to analyze the wettability of droplets on inkjet processes dynamically using molecular dynamics[12] or empirical models.[13] The predictability of these simulations strongly depends on the force fields that are currently prepared by empirical para-

Received: November 28, 2016
Published: October 5, 2017

DOI: 10.1021/acs.jctc.6b01159
J. Chem. Theory Comput. 2017, 13, 5217−5230

metrizations of Lennard-Jones type potentials. The *ab initio* assessment for these parametrizations is obviously recognized as an important breakthrough in getting more universal applicability.

For CHS, there is no reference to A, and then we tried evaluating A_{add} from its binding curve. Besides the anisotropy discussed above, the commonly available framework, DFT (density functional theory), is known to fail to describe molecular interactions mostly, and the DFT performance strongly depends on exchange-correlation (XC) functionals adopted.[14] In the present case, the interaction of this system, CHS, is of non-π staking nature, known as an *aliphatic*−*aliphatic* one[15] between the σ bonds at the HOMO (highest-occupied molecular orbital) levels of the monomers. Unlike $\pi-\pi$ interactions of, for example, benzene dimer, there has been only a few investigations on $\sigma-\sigma$ interactions and hence no established scheme of how to treat the anisotropy of molecules in the evaluation of binding curves even for moderately tractable size and symmetry of the target molecules. As is well-known, accurate correlated methods such as CCSD(T) are required to get enough reliable estimations of molecular interaction.[14,16] Such methods are, in general, quite costly in the sense of the scalability on the system size, N, for example, $\sim N^7$ for CCSD(T).[17] Such severe scalabilities obstruct the applications to larger molecules being likely in the practical cases. In contrast, DMC (diffusion Monte Carlo) method is quite promising, and its applicability to more practical issues gets rapidly extended.[18−21] This framework is regarded in principle as the most reliable that can achieve "numerically exact solutions" in some cases,[22,23] and there has been so far several applications to noncovalent systems,[24−34] to calibrate even over accurate molecular orbital methods such as CCSD(T). DMC scales at worst to $\sim N^3$,[19] making it possible to be applied further to larger molecules including molecular crystals.[29−33]

In this paper, we therefore applied DMC to evaluate A_{add} of CHS. Upon a careful benchmark on benzene molecule (given in Appendix C), we have established a scheme (i) coping with the anisotropy of the molecules, (ii) reducing statistical error bars and biases that are small enough for a usable predictions, and (iii) based on several possible validations on the predicted A for which no experimental reference value is available. The scheme is applied to CHS getting $A = 105 \pm 2$ zJ, which is in a reasonable range validated by several side considerations. By making comparisons with binding curves by DFT, we also provide a useful calibration over several XC for the predictability of A.

The paper is then organized as follows: In the main body of the paper, we provide descriptions of the scheme applied to CHS, followed by validations of the prediction and benchmarks for molecular systems with experimental values as briefly as possible so as to concentrate on following the established procedure. Thus, put aside into appendices are detailed descriptions for computational methods (Appendix A), some formalism of Hamaker constants considered in the present work (Appendix B), and all the discussions on the validations of the procedure made on the benzene dimer benchmark (Appendices C−E). Technical details about evaluation of A_{add} for CHS are also given alongside the benzene case in the appendices. Summaries of the paper are given as Concluding Remarks at the end of main text. Detailed correction schemes, such as BSSE (basis set superposition error), CBS (complete basis set) schemes, as well as time-step error in DMC, are given in Supporting Information.

RESULTS AND DISCUSSIONS

Hamaker Constant of CHS. To obtain C_6, we first evaluated dimer binding curves of CHS for three types of coalescences, that is, sandwich (type A), T-shape (type B), and parallel (type C), as shown in Figure 1. Computational details

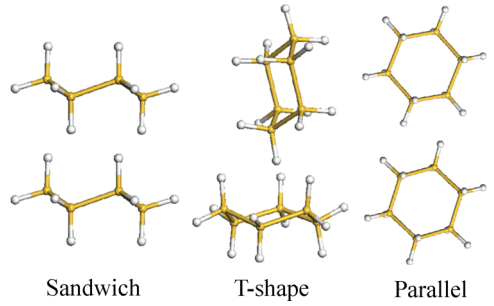

Figure 1. Typical configurations of the dimer coalescence considered in this work, sandwich (type A), T-shaped (type B), and parallel (type C).

for the evaluation are given in Appendix A. We took the chair conformation as the CHS monomer structure, because it is known to be most stable.[35,36] The monomer geometry is optimized at the B3LYP/6-311G level using Gaussian09.[37] To plot a binding curve, we vary binding distances of a dimer coalescence, leaving each of the monomer structures unchanged from the optimized ones. Here the intermonomer distance is defined as that between the centers of gravity of the monomers. The use of the fixed monomer geometries is valid to some extent because we focus on C_6 extracted from the long-range behavior where each of the monomer structures may be almost the same as that of an isolated monomer.

Figure 2 shows DMC binding curves for each of the coalescence configurations, compared with CCSD(T) references. The sandwich (type A) configuration is found to give the most stable binding energy, ΔE, over the others, $p \propto \exp(-\Delta E/(kT)) \approx 98\%$ at $T = 298.15$ K as given in Table 1. To obtain C_6 from the binding curves, we first evaluate the asymptotic exponents from the corresponding logarithm plots, as shown in Figure 3. The best fits of the exponents in DMC [CCSD(T)] give -5.6 ± 5.8 [-5.9], -4.2 ± 5.9 [-7.3], and -7.2 ± 7.2 [-8.7] for type A, B, and C, respectively. Supported by the CCSD(T) estimations, we can somehow find that type A dominates the wettability with the longest-ranged exponent that is close to the $\sim C_6/R^6$ dependence. For type A, we can then identify the C_6 constant from the fitting with exponent fixed to be 6.0. To sum up, only the stable configuration contributes to $\sim 1/R^6$ asymptotic behavior, while the others give different exponents. In addition to the above CHS case, our careful benchmark for the benzene case given in Appendix C clarifies that the deepest binding configuration almost dominates the Hamaker constants (the most stable coalescence, parallel displacement, asymptotically behaves as $\sim 1/R^6$, while the other ones do not). We can therefore concentrate only on the type A binding curve to extract C_6 from its asymptotic behavior. Hereafter we adopt a symbol, C_6^{stable}, as a C_6 value for the most stable coalescence configuration.

To extract C_6^{stable} from the PES data, we considered several fitting schemes: 6-12 Lennard-Jones (LJ) (Figure 2), log-fit

DOI: 10.1021/acs.jctc.6b01159
J. Chem. Theory Comput. 2017, 13, 5217−5230

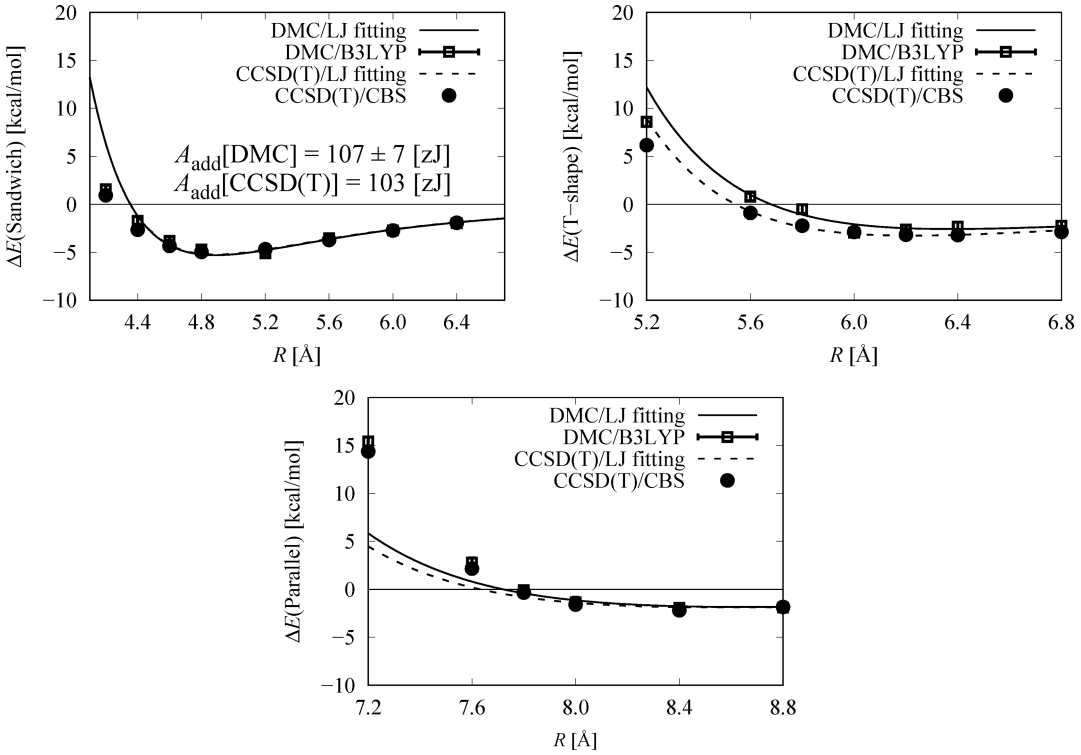

Figure 2. DMC binding curves for three types of coalescence (sandwich/T-shape/parallel) compared with CCSD(T). For eye-guide, Lennard-Jones fitting is depicted for both DMC and CCSD(T), though for T-shape and parallel, the fitting has a limited meaning because they do not behave like R^{-6} (see Appendix D for details).

Table 1. Comparisons of the Equilibrium Stability among Three Coalescence Configurations for CHS Shown in Figure 1, in Terms of the Thermal Probability Weight, $p \propto \exp(-\Delta E/(kT))$[a]

	B3LYP-GD3	MP2	CCSD(T)	DMC
p(A)/R_e	0.971/4.9	0.976/4.7	0.968/4.8	0.987(82)/4.83(2)
p(B)/R_e	0.026/6.6	0.023/6.1	0.030/6.2	0.010(24)/6.37(6)
p(C)/R_e	0.003/8.8	0.002/8.4	0.003/8.6	0.003(14)/8.7(1)
$\bar{R}_{dim}$	5.0	4.7	4.9	4.9(1)

[a]Equilibrium binding lengths, R_{eq} [Å], are also shown. $\bar{R}_{dim}$ [Å] is the thermal averaged binding lengths at T = 298.15 K for each method.

(Figure 3), and power-fit for the correlation energy defined as the deviation from Hartree−Fock energy (Figure 4), which are denoted as $C_6^{stable;LOG}$, $C_6^{stable;LJ}$, and $C_6^{stable;Corr}$, respectively. The estimation is also affected by the choice of which distance range is taken to be fit. We describe technical details of our fitting schemes in Appendix D, considering the benzene benchmark as well as CHS. From them, we find out that the power-fit for the correlation energy[38,39]

$$\Delta E_{corr}(R) = -\frac{C_6}{R^6} - \frac{C_8}{R^8} ... \quad (1)$$

achieves small enough error bars for usable predictions on the Hamaker constant by DMC, $A_{add}(C_6^{stable;Corr}) = 105 \pm 2$ zJ, with the fitting range R = 4.4−6.4 Å, which minimizes a measure of the deviation from the fitting model (Appendix D), where the experimental density of CHS, $\rho = 0.323 \times 10^{28}$[1/m^3] at 298.15 K,[40] was used to evaluate $A_{add} = \pi\rho^2 C_6$. The Hamaker constants evaluated from various approaches (methods/schemes) in the present study are listed in Table 2, and their validation is given in the next subsection.

Validation of *A* Value. We found that our DMC evaluations of A_{add} agree with those obtained from the other reliable quantum chemistry methods, CCSD(T) and MP2, implying our *ab initio* evaluation schemes would be reasonable within the framework of many-electron wave function theory. But, there is no reference to A to be compared directly to the present estimation for CHS. So we tried a validation via sideway manner as follows: (1) A simple evaluation based on London's theory[38] gives lower bounds of A_L, that is, it is well-known to underestimate A_L as well as A_{add} (See Appendix C for more detail).[3,41−43] Static polarizabilities and ionization energies were evaluated using HF and DFT levels of theory to give C_6 values (denoted as C_6^{London}), where the ionization energies are evaluated by the ΔSCF procedure. We found that HF gives $A_{add}(C_6^{London}) = 66$ zJ, while most DFT values give $A_{add}(C_6^{London}) \approx 80$ zJ. Note that HF underestimates the ionization energy significantly due to lack of correlation,[22] leading to HF underestimation of A_{add}. The London estimates with DFT are consistent in the sense that they are actually located in the underestimated range compared with the other estimations in Table 2.

(2) As another trial for the validation using the estimations (A_L) based on the Lifshitz theory,[44] whose formalism is given in Appendix B, we consider the dependence on the molecular weights of $A \propto C_6$. Since the dispersion interactions scale to the total polarization, expecting that A is roughly proportional to molecular weights is not so bad. Under this assumption, the ratio, $A_L(C_6H_{12})/A_L(C_5H_{10}) = (53.0 \pm 0.2)/(49.4 \pm 0.3)$, can be taken as being equal to $A_L(Si_6H_{12})/A_L(Si_5H_{10})$. Using the known value of A_L (73.4 ± 0.4 zJ) for CPS (Si_5H_{10}), we can roughly estimate that of CHS as A_L(extrapol.) = 78.9 ± 0.5 zJ. Another possible regression can be made in terms of C_6 instead of A. Regressing the quadratic functions to the TDDFT and

DOI: 10.1021/acs.jctc.6b01159
J. Chem. Theory Comput. 2017, 13, 5217−5230

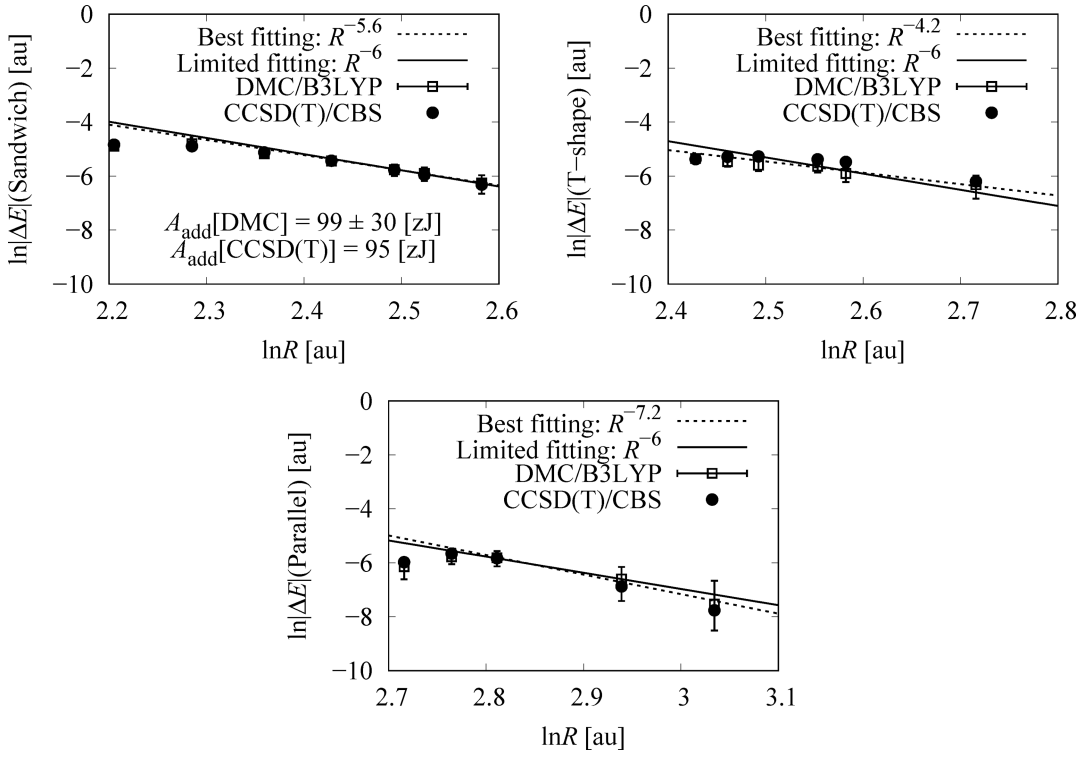

Figure 3. Asymptotic behaviors of binding curves evaluated by DMC and CCSD(T), as given in logarithmic plots fitted by two different lines, "Best" and "Limited". In the former fitting, the exponent is fitted to get the best fitting, while in the latter it is fixed to be assumed R^{-6} behavior.

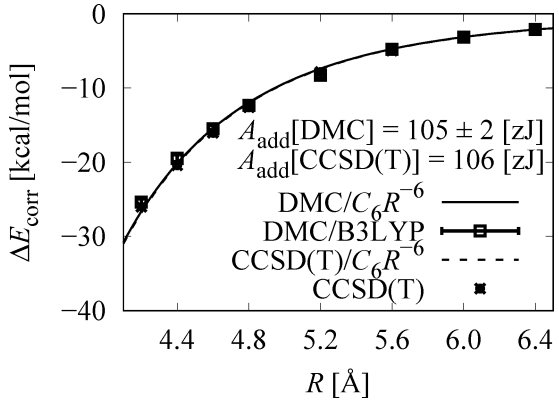

Figure 4. Correlation energy contributions to binding energies evaluated by DMC and CCSD(T).

EMT (effective medium theory) data on C_6 values of the Si_nH_m family[45] (denoted as $C_6^{extrapol.}$), we get $A_{add}(C_6^{extrapol.})$ = 110 zJ and 94 zJ, respectively. These values lie within a reasonable range by comparison with those in Table 2, being consistent with the fact that A_{add} is larger than A_L(extrapol.). We found the EMT extrapolation of A_{add} being closer to A_L(extrapol.). This may be attributed to the fact that, in EMT, C_6 is evaluated by the dielectric constants modeled by those of bulk quantities, as in the Lifschitz theory. The reason why A_{add} generally overestimates A values compared with A_L may be explained as follows: $A_{add}(C_6^{stable})$ is evaluated only from the longest-ranged exponent with a selected coalescence configuration, type A in the present case. The other configurations with shorter-ranged exponents should be included in liquids by some fractions, and hence effectively weaken the binding strength estimated under such an assumption with 100% constitution of type A coalescence. Such an effect would be represented as

Table 2. Computed Hamaker Constants, $A_{add}(C_6^{stable})$ [zJ], for CHS, based on Different C_6 Evaluation Schemes, $C_6^{stable;LOG}$, $C_6^{stable;LJ}$, and $C_6^{stable;\ Corr}$[a]

method/scheme	LOG	LJ	Corr	London
LDA	48	90	67	93
M06-2X	36	56	46	81
GGA-PBE				84
B3LYP				81
B3LYP-GD2	57	62	66	81
B3LYP-GD3	96	105	104	81
B97-D	98	81	101	82
HF				66
MP2	104	99	104	
CCSD(T)	95	103	106	
DMC	99(30)	107(7)	105(2)	

[a]See text for more details about the definitions. Since HF, PBE, and B3LYP give repulsive PESs, their Hamaker constants cannot be evaluated by the present PES scheme, and the London scheme is used to estimate $A_{add}(C_6^{London})$, instead. Statistical errors in the DMC values are given in parentheses.

"effectively reduced" Hamaker constants close to A_L. Hence, the values, A_{add}/A_L, could be sorted out by a factor dominating the fraction, $\exp(-\Delta E/(kT))$, where ΔE denotes a typical energy difference between the coalescence configurations with the longest- and the shortest-ranging exponents.

Validation of Equilibrium Properties. Although the long-range behavior of PES concerns the evaluation of A, validation of PES at equilibrium distance may also give us some confidence in our numerical results. Equilibrium properties including binding energies (ΔE) and equilibrium lengths (R_{eq}) are summarized in Table 3. The estimated binding energies in our DMC-PES are comparable with the typical value of non-π

DOI: 10.1021/acs.jctc.6b01159
J. Chem. Theory Comput. 2017, 13, 5217−5230

Table 3. Summary of the Abilities in Describing Each Binding Region at Various Levels of Theory[a]

	equilibrium properties			
	$\Delta E(R_e)$	R_e	short-range $\Delta E(4.2)$	long-range $\Delta E(7.0)$
LDA	−9.39 [NG]	4.34 [NG]	−8.73 [NG]	−0.44 [NG]
B3LYP-GD2	−3.47 [NG]	4.93 [G]	2.09 [NG]	−0.71 [NG]
B3LYP-GD3	−5.06 [G]	4.93 [G]	5.74 [NG]	−1.13 [G]
B97-D	−4.13 [NG]	4.88 [G]	2.73 [NG]	−1.24 [G]
M06-2X	−3.75 [NG]	4.67 [NG]	1.84 [NG]	−0.40 [NG]
MP2	−6.36 [NG]	4.70 [NG]	−0.88 [NG]	−1.23 [G]
DMC/B3LYP	−5.3(2) [G]	4.89(2) [G]	1.6(4) [G]	−1.2(4) [G]
CCSD(T)	−5.24	4.89	0.94	−1.13

[a]NG or G in brackets stands for No Good or Good, respectively. Statistical errors in the DMC results are indicated in parentheses.

stacking energies approximately −5 kcal/mol.[15] Compared with π-stacking energies, it is about two times larger, which would be consistent with the higher boiling temperature of CHS than that of its structural isomers with the same molecular weights but without hydrogen bonding.[46]

For further possible validations of our DMC-PES, we would take the facts that (a) the PESs are consistent with those estimated by another reliable standard, CCSD(T), and (b) we can make a plausible comparison that explains the experimentally observed density from our estimated binding lengths R_e. For point a, we shall make detailed discussions on the comparison as well with DFT later (see Calibration of DFT).

As for point b, we confirmed that our scheme that relating R_e with an experimental density works well for not only CHS but also benzene. For CHS, experimental values of the molecular weight (180.61 g/mol) and density (0.97 g/cm^3 at T = 298.15 K) lead to the mean intermolecular distance, $R_\rho \approx 6.8$ Å, which reasonably drops within the binding lengths of types A to C. As shown in Table 1, the simple thermal averaging over the three configurations by the factor $p \propto \exp(-\Delta E/(kT))$ underestimates R_ρ: $\overline{R}_{dim} \approx 4.9$ Å. An alternative averaging over four-body trapezoid configurations shown in Figure 5 gives an improved estimate, $\overline{R}_{tetra}$, getting closer to the experimental estimation of 6.8 Å, as shown in Table 4, where an "effective" length is measured as the square root of the trapezoid area. In the case of benzene, $\overline{R}_{dim} \approx 3.8$ Å and $\overline{R}_{tetra} \approx 5.0$ Å. The former

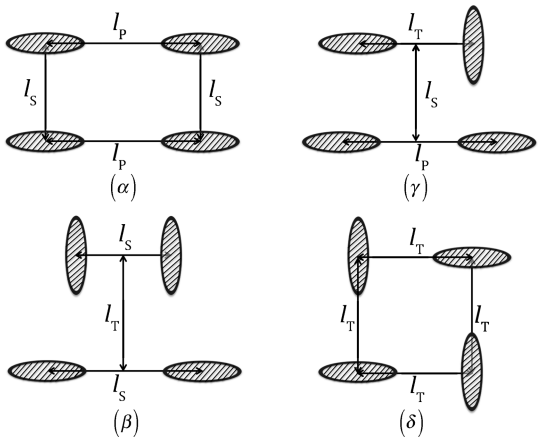

Figure 5. Possible four-body clusterings formed from the two-body coalescences shown in Figure 1. Hatched regions stand for the surfaces surrounded by the ring of cyclohexasilane molecule. l_S, l_T, and l_P correspond to the binding lengths with sandwich (type A), T-shape (type B), and parallel (type C) dimer configurations, respectively.

Table 4. Comparisons of the Equilibrium Stability among Four Clustering Configurations in Figure 5, in Terms of the Thermal Probability Weight, $p \propto \exp(-\Delta E/(kT))$[a]

	B3LYP-GD3	MP2	CCSD(T)	DMC
$p(\alpha)/R_\alpha$	0.343/6.6	0.293/6.3	0.327/6.4	0.48(27)/6.5
$p(\beta)/R_\beta$	0.243/6.7	0.248/6.3	0.245/6.5	0.21(7)/6.6
$p(\gamma)/R_\gamma$	0.243/6.6	0.248/6.1	0.245/6.3	0.21(7)/6.4
$p(\delta)/R_\delta$	0.172/6.6	0.210/6.1	0.183/6.2	0.09(19)/6.4
$\overline{R}_{tetra}$	6.6	6.2	6.4	6.5(2)

[a]ΔE is computed from a sum of dimer pairs in the tetramer. $R_{\alpha,\beta,\gamma,\delta}$ [Å] are the effective lengths for tetramers, α, β, γ, δ (see text), and $\overline{R}_{tetra}$ [Å] is their thermal averaged length at T = 298.15 K. Statistical errors in DMC are given in parentheses.

underestimates and the latter agrees with an experimental estimation of $R_\rho \approx 5.3$ Å (For detail, see Appendix E).

Calibration of DFT. DFT is a much more practical choice of methods combined with our *ab initio* Hamaker evaluation schemes, but its reliability strongly depends on XC functionals adopted as usual. Here we provide a useful calibration over several XC functionals appropriate for predicting A values, by comparing with the many-electron wave function theories.

Figure 6 highlights typical binding curves evaluated by various methods, though only for type A (for the other types, see Supporting Information). All the SCF curves were corrected by the BSSE scheme[17,47−49] (see Supporting Information). The present study takes CCSD(T) as a standard reference to calibrate the performance of the SCF approaches. We can find the DFT predictions scattering around CCSD(T). Except LDA, conventional functionals such as PBE and B3LYP fail to capture the binding itself. The LDA overbinding has been frequently reported for a number of molecular systems.[29−32,50] This can be regarded as spurious due to improper self-interactions: exchange repulsion is not fully reproduced in LDA because of the lack of the exact cancellation of self-interaction, and hence spurious "chemical" bindings are formed due to the weakened repulsions, rather than true chemical bindings. The exchange repulsion weakened in LDA gets recovered when changing XC into GGA and further into B3LYP, which may explain the repulsive curves pushing the minimum toward distant region. As LDA is known to inherently fail to describe dispersion interactions, a significant difference in the LDA estimations between $A_{add}(C_6^{stable;LOG})$ and $A_{add}(C_6^{stable;LJ})$ (see Table 2) implies a poor reliability on its long-range behavior description.

The XC functionals for molecular interactions, M06-2X, B97-D, and B3LYP-GD(2,3), on the other hand, well reproduce the bindings at their equilibrium lengths, as seen in Figure 6. We

DOI: 10.1021/acs.jctc.6b01159
J. Chem. Theory Comput. 2017, 13, 5217−5230

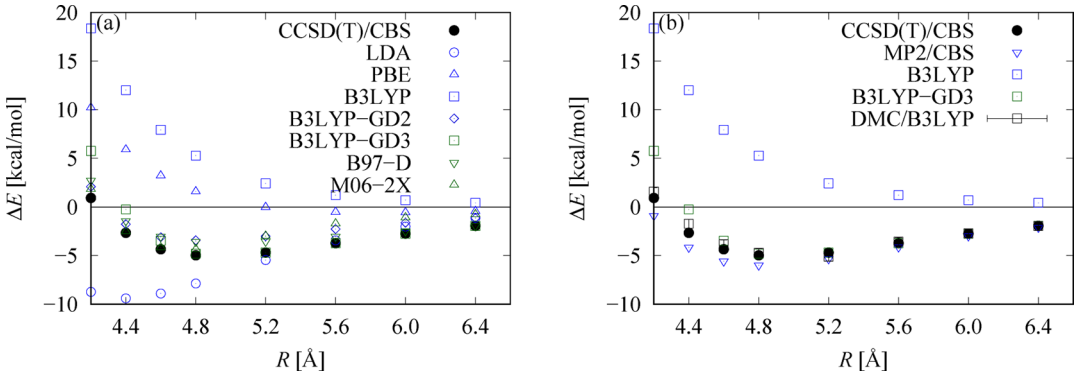

Figure 6. Binding curves of type A (sandwich) dimer coalescence evaluated by (a) DFT methods (LDA, PBE, B3LYP, B3LYP-GD2/GD3, B97-D, M06-2X) and (b) correlation methods (MP2, CCSD(T), and DMC/B3LYP) compared with selected DFTs. All the curves (except DMC) are corrected by BSSE and CBS (see Supporting Information for more details).

see, however, that M06-2X and B3LYP-GD2 give rise to less reliable asymptotic behaviors at long-range region, where they decay much faster than CCSD(T) or the other XC functionals for molecular interactions. As for M06-2X, its functional form based on hybrid meta-GGA does not explicitly contain dispersion interactions by its construction, and its parametrizations of the XC functionals are adjusted so as to reproduce a number of molecular bindings *around* their equilibrium geometries, giving rise to the unreliable long-range behavior. B97-D and B3LYP-GD2 are classified into the DFT-D2 family including "atom-pairwise" second-order perturbative dispersion corrections (two-body term).[51] Both B97-D and B3LYP-GD2 give poor estimates of binding energies and lengths, but the former behaves better than the latter at long-range region, being appropriate for the estimation of Hamaker constants. This implies long-range behaviors also depend on original functionals, and atom-pairwise dispersion corrections do not necessarily lead to a correct description of "molecule-pairwise" dispersion interactions, as in the B3LYP-GD2 case. It has been reported that DFT-D3 including atom-pairwise third-order perturbative dispersion corrections (three-body term) can remedy this kind of discrepancy in long-range as well as equilibrium behaviors at the DFT-D2 level of theory.[52] It is notable that the present B3LYP-GD3 binding curve is well improved in its long-range behavior to reproduce a correct decaying exponent. For the present CHS case, its correct molecule-pairwise dispersion behavior at long-range region requires both the second- and third-order perturbative dispersion corrections. Looking at the short-range region, on the other hand, we find that B97-D and M06-2X give a better description than B3LYP-GD3, getting closer to the DMC and CCSD(T) estimations. This suggests that B3LYP-GD3 includes too large Hartree−Fock exchange effects to be adequately canceled out by correlation effects. The above results can be summarized in Table 3.

Our DMC and MP2 results are shown in Figure 6b, compared with the reference CCSD(T), the typical SCF (B3LYP), and the best within DFT at equilibrium and long-range regions (B3LYP-GD3). As is well-known, MP2 overbinds with deeper (shorter) binding energy (distance).[53] It may not be surprising to get the coincidence of asymptotic behaviors between MP2 and CCSD(T), because the present CCSD(T) is corrected by the CBS scheme taken from MP2[54] (see Supporting Information). Three DMC curves were obtained starting from guiding functions generated by LDA, PBE, and B3LYP, respectively (see Supporting Information). They almost converged to the same binding curve, even starting from either B3LYP (worst in reproducing binding at SCF level) or LDA (too deep spurious overbinding at SCF level). Similar insensitivity to the choice of guiding functions has been also reported for a DNA stacking case,[29] implying that these DMC predictions are not seriously affected by the fixed-node approximation. Based on the variational principle with respect to nodal surfaces in DMC,[55−57] we henceforth concentrate on the B3LYP guiding function only, because it gives the lowest total energy though the energy differences among the three binding curves are quite small. Note that this is consistent with a number of previous DMC studies.[29,58−61]

The present DMC is found to give almost the same results as CCSD(T). A remarkable difference between CCSD(T) and DMC is the binding energy at short-range, $\Delta E(4.2)$ by ∼0.6(±0.4) kcal/mol. The difference would be partly attributed to the dynamical correlation effect, which becomes more important at shorter binding length as well as exchange repulsions. Even under the fixed-node approximation, the dynamical correlation is expected to be well described,[18,19,24−32] and hence the present DMC curve is regarded as the best description of the binding of CHS.

Benchmarks. The scheme shown to work for CHS might look somewhat arbitrary, as no experimental reference is known. To make this more convincing, we would need to show the scheme also works for a couple of systems where the experimental values are known. Table 5 summarizes the results of such benchmarks, using several methods applied to C_6H_6 and C_6H_{12}. In these estimations, we considered parallel displacement and sandwich configurations for C_6H_6 and C_6H_{12}, respectively. Our A_{add} values based on the scheme are found to agree well with experimental ones, A_L, albeit with

Table 5. Computed Hamaker Constants, $A_{add}(C_6^{stable})$ [zJ], Based on Different C_6 Evaluation Schemes, $C_6^{stable;LOG}$, $C_6^{stable;LJ}$, and $C_6^{stable;Corr}$[a]

molecule	method	LOG	LJ	Corr	expt
C_6H_6	DMC	54(12)	51(4)	*b*	50(2)
C_6H_{12}	B3LYP-GD3	70	82	72	53(2)
	MP2	81	78	83	
	CCSD(T)	71	72	73	

[a]See text for more details about the definitions. Statistical errors in the DMC values are given in parentheses. Experimental values for C_6H_6 and C_6H_{12} were both evaluated from ref 62. [b]Not applicable.

DOI: 10.1021/acs.jctc.6b01159
J. Chem. Theory Comput. 2017, 13, 5217−5230

some overestimation. This is the same tendency as discussed in the section entitled Validation of A Value. The smaller discrepancy with experiments for the smaller size of molecule would be accounted for as follows: As discussed in the previous section, the major origin of the discrepancy comes from the anisotropy, which cannot be well captured by the $A_{add}(C_6^{stable})$ scheme. Since the anisotropy generally gets larger when the molecular size gets larger, the discrepancy is expected to get larger as well.

Practicality: DMC vs CCSD(T). Figure 7 shows the comparison between DMC and CCSD(T) with and without

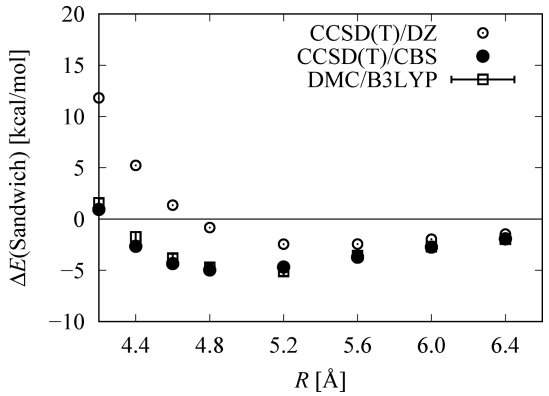

Figure 7. Comparison of binding curves between DMC and BSSE-corrected CCSD(T) with the CBS/DZ basis set. "CCSD(T)/DZ[CBS]" stands for the raw value without any corrections by DZ basis sets [CBS limit], while "BSSE-CCSD(T)/DZ[CBS]" means that with BSSE corrections.

basis set (CBS) corrections. Even though CCSD(T) is known as the "gold standard" among *ab initio* predictions, the practical use of CCSD(T) requires very careful handling of corrections, as described in Supporting Information, to get enough reliable predictions.[63] The correction itself is also under quite a limited approximation[54,64] (see eq 1 in Supporting Information). These practical limitations are, in contrast, not the case in DMC because it is free from the basis set choice to the extent that only the nodal structure of the many-body wave function is fixed by the given basis set. In order to evaluate Hamaker constants of practically larger systems, therefore, DMC has the advantage over CCSD(T) in the sense of less sensitivity to basis sets.

We have to note, in fairness, that the preparation of *workable* DMC trial wave functions would be far from straightforward in practice. Though, in principle, DMC predictions are not relying on the choice of trial wave function (except nodal surfaces), no acceptable numerical stabilities and significant statistics are achieved without carefully brushed up trial wave function via VMC optimizations.[65] Once the optimization has been achieved, it is true to take advantage of $\sim N^3$ scaling over CCSD(T), though the optimization procedure sometimes exhausts human and computational resources. This is in contrast to rather transparent procedures for basis sets in CCSD(T).

Our proposed scheme begins with the landscape of binding curves to find that of the most stable configuration, from which asymptotic behaviors are extracted. For this purpose, it is still helpful to use quick DFT evaluations, though one should be careful for the choice of XC functionals. As shown in Tables 2 and 3, it was found that at least GD3 level of theory for dispersion is necessary for obtaining reliable evaluations of both equilibrium and asymptotic properties.

Table 6 summarizes the comparison of computational costs using several methods. Though the apparent expensiveness of

Table 6. Computational Costs for Several Methodologies in Terms of Core-Hour, Which Is CPU Time Multiplied by the Number of Cores Exploited[a]

method	cost [core-hour]
B3LYP-GD3/CBS	9
MP2/CBS	34
CCSD(T)/cc-pVDZ	159
CCSD(T)/CBS	183
QMC (=opt.+DMC)	1587 (=9 + 1578)

[a]Note that CCSD(T)/CBS equals a sum of CCSD(T)/cc-pVDZ and MP2/CBS.

QMC may attract attention, we note that the achieved accuracy and reliability are not the same: CCSD(T)/CBS is around 1/9 times cheaper than QMC; the reliability is assured up to cc-pVDZ basis set level. While further refinement about the basis set is not feasible by the current computational resources, we can fully utilize quite a high parallel efficiency of QMC[32] to speed up. We note that the unit in Table 6 is core-hour, and the current parallel implementation of CCSD(T) works up to around 16 parallel processes.[66] It is practically even in the sense of required elapse time between QMC and CCSD(T) by using 640-core parallel environment, which is now commonly available in the middle scale computational facilities.

CONCLUDING REMARKS

We considered a scheme using DMC-PES to evaluate Hamaker constants A for practical anisotropic molecules and applied it to a cyclohexasilane (CHS) molecule used as an ink for printed electronics. The scheme should take into account two important factors for practical applications, namely, the weak molecular interactions dominated by electron correlations (especially dispersion) and nonunique coalescing direction between anisotropic molecules. By making comparisons with the estimations by the Lifschitz theory (A_L) on benzene, we clarified several possible origins to give systematic biases on A_{add} when it is estimated by PES with or without any averaging operations over anisotropy. The success of our scheme in the benzene case leads us to its application to CHS. In the application to CHS, our DMC results coincide fairly well with other correlation methods such as CCSD(T), MP2, and several DFT with exchange-correlation functionals for molecular interactions, like B3LYP-GD3. The evaluated binding curve can be reasonably validated by the experimentally observed density of the liquid solution via a scheme to relate its binding length and the mean intermolecule distance. We find out that the parallel-wise coalescence of molecules gives the longest distant exponent for the interaction, being around 6.0. Several possible fitting schemes are applied to get A_{add}, and finally we estimate it around 105 ± 2 zJ, with practically enough small statistical error. Though there is no experimental data available for a direct comparison, the present estimation is well supported from the trend of both Hamaker constants for similar kinds of molecules and systematic difference between the predictions by the Lifshitz theory and by the asymptotic exponent estimations.

DOI: 10.1021/acs.jctc.6b01159
J. Chem. Theory Comput. 2017, 13, 5217−5230

APPENDIX A. COMPUTATIONAL METHODS

The binding curves are evaluated by DMC, compared with CCSD(T), MP2, and several DFT calculations with various XC functionals. As a common choice, the fixed-node approximation[18,19] was made to the DMC simulations (DMC), taking Slater−Jastrow wavefunctions as the guiding functions. The Slater determinants are composed of Kohn−Sham (KS) orbitals obtained using Gaussian09[37] with Burkatzki−Filippi−Dolg (BFD) pseudopotentials (PP)[67] and its accompanying VTZ Gaussian basis sets. The BFD-PPs have been proven to give enough practical accuracies not only in DMC but also in DFT on applications such as a DNA stacking problem.[29]

Our Jastrow functions[68,69] were those implemented in CASINO,[18] consisting of one-, two-, and three-body contributions, denoted as χ-, u-, and F-terms, respectively. The χ-, u-, and F-terms include 16, 16, and 32 adjustable parameters, respectively. They were optimized by the variance minimization scheme.[70,71] The electron−electron cusp condition[72] was imposed only on the u-term during the optimization procedure. For DMC statistical accumulations, we set the target population (the number of random walkers) to be 1024 configurations on average and the time step to be $\delta t = 0.02$ in atomic unit. The time step bias[73] arising from this choice is discussed in Supporting Information. We took averages over 1.7×10^5 accumulation steps after the equilibration of 10^3 steps. We also used T-move scheme[57] for the locality approximation to the evaluation of PPs[55,56] in DMC.

Only for type A, we benchmarked various DFT-SCF calculations for a comparison with DMC, seeing how the choice of the XC functionals affects the trial nodal structures in DMC. Our choice of XC functionals in DFT includes those recently designed for molecular interactions, B3LYP+GD2[51]/GD3,[52] M06-2X,[74] and B97-D,[51] as well as LDA,[75] PBE,[76] B3LYP.[77−79]

For a systematic comparison, we consistently used the same basis sets as DMC, VTZ basis sets provided in BFD-PP library.[67] For correlated methods (MP2 and CCSD(T)), however, the VTZ is too large to be accommodated in tractable memory capacities (512 GB shared by 64 parallel cores in SGI Altix UV1000). To correct biases due to basis set choices, we considered Complete Basis Set (CBS) methods[54,64] with two different basis sets, and counterpoise methods for basis set superposition error (BSSE).[17,47−49] Detailed discussions about these corrections are given in Supporting Information. All the DFT-SCF and correlated calculations were performed using Gaussian09.[37]

As demonstrated in Supporting Information, all the three functionals give almost the same binding energy and equilibrium distance, but B3LYP is found to give the best nodal surface in the sense of the variational principle. Hence we concentrated only on B3LYP orbitals for DMC for type B and C.

APPENDIX B. SUMMARY OF FORMALISMS OF HAMAKER CONSTANTS

In most practical cases, the Hamaker constants are estimated by the macroscopic frameworks based on the Lifshitz theory[44] (let us denote the estimation by these frameworks as A_L). In the scheme $A_{add} = \pi C_6 \rho^2$, several possibilities are available for C_6 evaluations, including those (i) by DOSD (dipole oscillator strength distribution) experiments,[41] (ii) by estimations by the Casimir−Polder relation (CPR)[80] using *ab initio* evaluations of dynamical polarizabilities,[42,43] and (iii) by the fitting of asymptotic behaviors in the molecular binding curves or potential energy surfaces (PES), evaluated by *ab initio* calculations.[81] The Casimir−Polder formula for option ii is given in hartree units as

$$C_6 = \frac{3}{\pi}\int_0^\infty \mathrm{d}u\ \bar{\alpha}(iu)^2 \tag{2}$$

in an integral over the imaginary frequency, iu, of the orientation average of the polarization tensor, $\bar{\alpha}(iu) := (1/3)\mathrm{Tr}[\alpha(iu)]$. $\bar{\alpha}$ can be evaluated by TDDFT (time-dependent DFT) within the linear response theory.[42,43] Provided that the molecule has a unique absorption frequency (ionization energy), ν_I (= I/h), a further approximation with $\bar{\alpha}(iu) \approx \bar{\alpha}(0)\nu_I^2/(u^2 + \nu_I^2)$ substituted to (eq 2) leads to the London formula of the dispersion force,[38]

$$C_6 = \frac{3}{4}\bar{\alpha}^2(0)I \tag{3}$$

where $\bar{\alpha}(0)$ is the static polarizability.

C_6 for practical anisotropic molecules obviously depends on the orientation of coalescence, such as T-shape, parallel, or sandwich. Plausible averaging is required over the possible orientations to get A_{add}, which is the main subject of the present study. This would be a reason that A_L is used much rather than A_{add} because in the former the nonadditivity as well as the anisotropy are effectively taken into account by using macroscopically averaged quantities. In options i and ii, the macroscopic or observed quantities used in the formula would be regarded as the effective consideration of such averaging to give $\langle C_6 \rangle$, as we used in Table 7. For most of the practical cases, the Hamaker constants are evaluated not by A_{add} but by A_L, a macroscopic framework based on the Dzyaloshinskii−Lifshitz−Pitaevskii (DLP) theory, in which the Hamaker constant is

Table 7. Comparisons of Hamaker Constants, A, of Benzene Estimated by Different Schemes[a]

label	scheme/theory/method	C_6, 10^3 [au]	A [zJ]
$1/A_L$	Exp/DLP	NA	50 ± 2[b]
$2/A_{add}(\langle C_6^{London}\rangle^{iso})$	London/HF	0.925[c]	42
$3/A_{add}(\langle C_6^{London}\rangle^{iso})$	London/B3LYP	1.105[d]	48
$4/A_{add}(\langle C_6^{CPR}\rangle^{iso})$	CPR/TDHF	1.737[e]	75
$5/A_{add}(\langle C_6^{CPR}\rangle^{iso})$	CPR/TDDFT	1.773[f]	77
$6/A_{add}(\langle C_6^{DOSD}\rangle^{iso})$	Exp/DOSD	1.723[g]	74
$7/A_{add}(C_6^{PES})$ (sandwich)	PES/MP2	0.59[h]	25
$8/A_{add}(C_6^{PES})$ (sandwich)	PES/CCSD(T)	0.602[i]	26
$9/A_{add}(C_6^{PES})$ (T-shape)	PES/CCSD(T)	3.911[i]	169
$10/A_{add}(\langle C_6^{PES}\rangle^{iso})$	PES/DFT-SAPT	1.726[j]	74
$11/A_{add}(\langle C_6^{PES}\rangle^{iso+aniso})$	PES/DFT-SAPT	1.165[k]	50
$12/A_{add}(C_6^{PES})$ (ParaDisp)	PES/DMC/log	1.25 ± 0.27[l]	54 ± 12
$13/A_{add}(C_6^{PES})$ (ParaDisp)	PES/DMC/LJ	1.19 ± 0.10[l]	51 ± 4

[a]The braket, $\langle\cdots\rangle$, means spatial averaging (see text for details). [b]Reference 3. [c]Ionization energy and static polarizability were obtained at HF/6-311++G(3d,3p) level. [d]Ionization energy and static polarizability were obtained at B3LYP/cc-pVQZ level. [e]Reference 42. [f]Reference 43. [g]Reference 41. [h]Reference 84. [i]Reference 54. [j]Reference 81. [k]This work with data from ref 81. [l]This work with data from ref 85.

DOI: 10.1021/acs.jctc.6b01159
J. Chem. Theory Comput. 2017, 13, 5217−5230

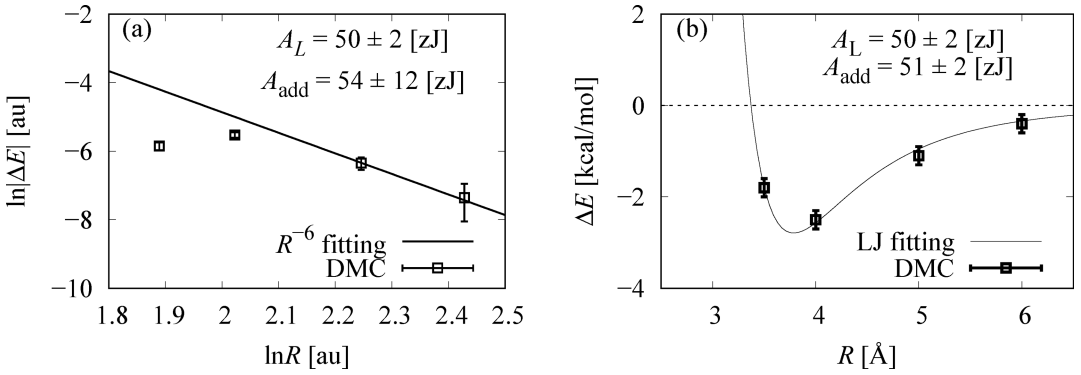

Figure 8. DMC binding curves of benzene dimer: (a) logarithmic plot fitted by asymptotic R^{-6} behavior and (b) Lennard-Jones fitting.

expressed as an infinite series of an expansion. Truncation up to the second term gives a practical approximation, known as Ninhan−Parsegian formula,[82,83]

$$A_L = \frac{3}{4}kT\left(\frac{\varepsilon - 1}{\epsilon + 1}\right)^2 + \frac{3h\nu_e}{16\sqrt{2}}\frac{(n^2-1)^2}{(n^2+1)^{3/2}} \quad (4)$$

and its truncation error is estimated to be around 5%.[3] The Hamaker constant can then be evaluated using macroscopic quantities of the bulk, that is, dielectric constant, ε, and the refractive index, n (k and T are the Boltzmann constant and absolute temperature, respectively, while h and ν are the Planck constant and the frequency of the primary electronic excitation in ultraviolet range). Unlike A_{add}, the macroscopic A_L can avoid the additive assumptions, namely, the macroscopic quantities effectively take into account the nonadditivity as well as the anisotropy.

APPENDIX C. COMPARISON OF DIFFERENT PREDICTIONS OF *A*

For the side-way manner of the validation of A predicted for CHS, we would like to know if there is a systematic bias between A_{add} and other macroscopic A_L. For this purpose, we take benzene as a representative tiny benchmark. In this case, there are many references to C_6 and A_L available in literature,[3,41−43,81] by which we can survey the possible relation between A_{add} and A_L to get a plausible validation for the estimate of realistic Hamaker constants $A_{add}(C_6)$ evaluated from *ab initio* PES calculations. Even for this simple molecule, there has been little investigation relating it to A_{add} for practical molecules, though it is straightforward. This might be attributed to the difficulty of the averaging over anisotropic configurations of coalescence.

Table 7 summarizes the Hamaker constants estimated by several approaches explained in Appendix B. Nos. 2−6 in Table 7 are obtained using C_6 evaluated by London's theory, CPR, and DOSD, which can be regarded as an equivalent averaging over orientations to get a representative isotropic value, $\langle C_6\rangle^{iso}$. For London's theory (nos. 2 and 3), the closer values to A_L (no. 1) might be accidental. These should be comparable rather to nos. 4 and 5 but turned out to be underestimated by around 40%. The underestimation can be explained because, as we mentioned, the London theory only picks up single absorption frequency, ignoring other contributions, which are all positive. Nos. 4−6 are consistent with each other being around 75 zJ, but overestimating when we take A_L as the reliable reference for the perfect averaging about the anisotropy and nonadditivity. The importance of the anisotropy can be seen in Nos. 7−9, where C_6 are evaluated only by PES for a coalescence configuration, such as sandwich or T-shape. We see that different methods for PES give consistent results with each other for the same configuration (no. 7 and no. 8), while the same method gives a different estimation for different configurations (no. 8 and no. 9).

SAPT evaluations, no. 10 and no. 11, give some confidence about the effective isotropic averaging for nos. 4−6 and the importance to consider the anisotropy for the A_L value. In SAPT, the dispersion interaction is evaluated in the form,

$$E_{disp} \approx -\frac{1}{R^6}\sum_{l_A,k_A,l_B,k_B,l} C_6[l_A, k_A, l_B, k_B, l]w_6 [l_A, k_A, l_B, k_B, l](\omega_A, \omega_B, \Omega) \quad (5)$$

as the summation over the possible anisotropic configurations labelled by the rank of tensor $\{l_A,k_A,l_B,k_B,l\}$ with each weight w_6. $\{\omega_A,\omega_B,\Omega\}$ denote the Euler angles between molecules A and B, and the solid angle between the molecules, respectively. No. 10 is evaluated from the isotropic contribution, $C_6[0,0,0,0,0] = 1726$, and consistent with nos. 4−6 as expected. We can also obtain the anisotropic contributions from the supplemental information of ref 81, $C[0,0,2,0,2] = C[2,0,0,0,2] = -552$, $C[2,0,2,0,0] = 17$, $C[2,0,2,0,2] = 45$, $C[2,0,2,0,4] = 482$, to estimate no. 11. To avoid the complicated averaging operations with serious weightings, we simply take the arithmetic mean for isotropic and anisotropic contribution and get $\langle C_6\rangle^{iso+aniso}$ quite closer to A_L in no. 1.

Nos. 12 and 13 give the estimation by a single configuration, parallel-displacement (ParaDisp), which is identified as the most stable binding.[86] The estimation is made from the DMC data by Azadi et al.,[85] from which we fit C_6 using log plots (no. 12) or 6-12 Lennard-Jones (LJ) potential (no. 13) as shown in Figure 8. Since we are interested in the long-range asymptotic behavior $\sim R^{-6}$, we did not take the original spline-like fitting function used in ref 85, which is used to describe the whole PES shape being different from the present purpose. We note for the log plot that the larger error bar is a sort of inevitable consequence of log-plot for long-range exponents.[8] For a fixed magnitude of statistical errors over the range of distance R, any decreasing dependence on a log-plot gives inevitably enlarged error bars as R increases (the resolution of the vertical axis gets enlarged downward by *definition*). In the present case, the statistical noise has been well suppressed, less than 0.02 kcal/mol, and further reduction of the error bar in A is not practical. In LJ fitting, on the other hand, enough practical reduction of the error bar has been achieved. The estimation of the fitting

DOI: 10.1021/acs.jctc.6b01159
J. Chem. Theory Comput. 2017, 13, 5217−5230

actually depends on the choice of the details of fitting functions and data range of the fitting, which we have chosen carefully with some validation as shown in Appendix D. Despite a single configuration, the fitting for the parallel-displacement configuration, nos. 12 and 13, coincides well with A_L. This implies that the most stable binding configuration (parallel displacement in this case) is almost dominant, and other possible configurations can be ignored for A.

APPENDIX D. FITTING SCHEME FOR C_6

Several different fitting schemes are possible to extract C_6 from PES, in principle, such as log-fit ($C_6^{\text{stable;LOG}}$), LJ-fit ($C_6^{\text{stable;LJ}}$), and the power-fit for the correlation contribution ($C_6^{\text{stable;Corr}}$). Table 8 summarizes the fitting results of benzene using various kinds of fitting functions and the choices of data range to be fit. While every fitting seems to work fairly well as shown in Figure 9, the estimations of A significantly depend on the arbitrary choice. We tried 6-12 LJ, 6-9 LJ, 6-exponential potential (6-exp),[87] and pairwise polynominal fitting function.[85] The choice of the fitting range is about whether we include the data at repulsive region (at R = 3.0) or not. Only for 6-exp we could not get reasonable convergence without the data point at R = 3.0 to increase the data points for such a strong nonlinear fitting. For the polynominal, we could not extract C_6 for the asymptotic R^{-6} behavior as we mentioned in the previous paragraph, but we can use it to get a reliable reference for the binding energy, ΔE, and bonding length, R_e, as it is the most precise function for the whole fitting purpose as described in ref 85. Taking those references for ΔE and R_e, we see that excluding the repulsion point, R = 3.0, from LJ fitting gives better estimations. Though the log-fitting result (no. 12) in Table 7 has the large error bar, the value is reliable to some extent in the aspect of the asymptotic behavior, from which 6-9 LJ (3.5−6.0) gives larger deviation. Based on these facts, we finally take 6-12 LJ (3.5−6.0) to provide the value no. 11 in Table 7.

Table 8. Dependences of Estimated Binding Energies (ΔE), Binding Lengths (R_e), and Hamaker Constants (A_{add}) on the Choices of Fitting Functions and Fitting Ranges

functions	range	ΔE [kcal/mol]	R_e [Å]	A_{add} [zJ]
6-12 LJ	3.0−6.0	−2.4 ± 0.2	3.54 ± 0.01	29 ± 2
6-12 LJ	3.5−6.0	−2.8 ± 0.2	3.78 ± 0.02	51 ± 4
6-9 LJ	3.0−6.0	−2.4 ± 0.2	3.64 ± 0.01	52 ± 3
6-9 LJ	3.5−6.0	−2.6 ± 0.2	3.81 ± 0.03	76 ± 7
6-exp	3.0−6.0	−2.5	3.88	70 ± 11
pairwise poly.[85]	3.0−6.0	−2.7 ± 0.3	3.8 ± 0.3	[a]
CCSD(T) reference[b]				
configuration		ΔE	R_e	
PD (most stable)		−2.78	3.87	
T-shape		−2.74	5.01	
sandwich		−1.81	6.09	

[a]Not applicable. [b]Reference values for ΔE and R_e by CCSD(T) are also shown, obtained from ref 54.

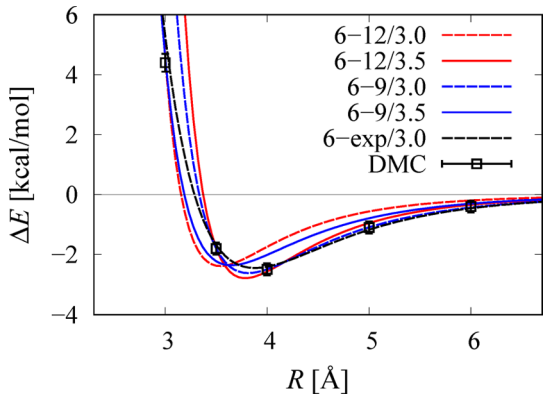

Figure 9. Comparison between different fitting schemes of DMC binding curves (benzene dimer with parallel-displacement (PD) configuration) using 6-12 LJ (Lennard-Jones), 6-9 LJ, and 6-exp with different fitting ranges (e.g., "6-12/3.0" means the range starting from R = 3.0 Å).

For CHS, the results using different fitting schemes were tabulated in Table 2 of main text. We start with the log-fit ($C_6^{\text{stable;LOG}}$). To obtain plausible estimates of $C_6^{\text{stable;LOG}}$, it is essential to choose their fitting region, R_f, at long-range. We focus on the relation that by definition the binding energy can be decomposed as the sum of Hartree−Fock (HF) and correlation contributions: $\Delta E(R) = \Delta E_{HF}(R) + \Delta E_{corr}(R)$.[88] Since $\Delta E_{HF}(R)$ (exponentially) decays much faster than $\Delta E_{corr}(R)$ (polynomially) at large R, the asymptotic behavior is dominated by $\Delta E_{corr}(R)$. Thus, we choose R_f such that $R \in R_f$ satisfies $|E_{HF}(R)/E_{corr}(R)| < 1/10$. As mentioned in the main text, we found only type A has $\sim 1/R^6$ asymptotic behavior (see Figure 3 of main text), which is the most stable configuration. On the other hand, the other configurations have weaker contributions to long-range behaviors. Note that this "less contributions to A" from other metastable configurations is quite in contrast to the case for the molecular density estimation, for which only the stable binding configuration cannot reproduce the proper density, as described in Appendix E.

As was explained in the benzene case, the log-fits are inevitably accompanied by the larger statistical error bars. If we aimed to reduce the error bar by one more digit, 100 times more statistical accumulation would be necessary. This computation corresponds to 2.2×10^6 core-hours (half a year CPU time on 512 cores parallel, provided that we can keep on using it without any queue) and hence is impractical.

The larger error bars in the log-fitting are much improved by using the other fitting schemes: The present study employed the 6-12 LJ fitting (Figure 2 of main text) using

$$U(R) = -\frac{C_6}{R^6} + \frac{C_{12}}{R^{12}} \tag{6}$$

and the correlation fitting (Figure 4) based on a power expansion,[38,39]

$$\Delta E_{corr}(R) \approx -\frac{C_6}{R^6} \tag{7}$$

to extract C_6 from PES. As was discussed in the benzene case, the estimation depends on the data fitting range, and then some plausible choice is required. Table 9 compares the choices especially about whether the range includes repulsive region (R < 4.4). To get the best choice, we adopted a figure of merit,

$$f = \sum_{j=1} \frac{(\Delta E(R_j) - U(R_j))^2}{\sigma(R_j)^2} \tag{8}$$

as defined using the deviation of $\Delta E(R_j)$ from the fitting, weighted by the statistical error $\sigma(R_j)$ in DMC [which is set to

DOI: 10.1021/acs.jctc.6b01159
J. Chem. Theory Comput. 2017, 13, 5217−5230

Table 9. Dependence of the Hamaker Constant, A_{add}, on Types of Fitting Functions, $U(R)$, Fitted within Ranges R_f for DMC and CCSD(T)[a]

method	$U(R)$	R_f	ΔE	R_e	A_{add}	f
DMC	6-12 LJ	4.2−6.4	−4.9 ± 0.2	4.74 ± 0.01	85 ± 4	1.198
	6-12 LJ	4.4−6.4	−5.2 ± 0.2	4.79 ± 0.01	100 ± 5	0.113
	6-12 LJ	4.6−6.4	−5.3 ± 0.2	4.89 ± 0.02	107 ± 7	0.033
	6-12 LJ	4.8−6.4	−5.2 ± 0.2	4.96 ± 0.03	112 ± 9	0.206
	Corr.	4.2−6.4			103 ± 1	0.022
	Corr.	4.4−6.4			105 ± 2	0.005
	Corr.	4.6−6.4			108 ± 2	0.020
	Corr.	4.8−6.4			110 ± 5	0.062
CCSD(T)	6-12 LJ	4.2−6.4	−5.10	4.76	86	0.027
	6-12 LJ	4.4−6.4	−5.27	4.82	95	0.004
	6-12 LJ	4.6−6.4	−5.24	4.89	103	0.002
	6-12 LJ	4.8−6.4	−5.12	4.94	107	0.006
	Corr.	4.2−6.4			106	0.018
	Corr.	4.4−6.4			108	0.034
	Corr.	4.6−6.4			110	0.053
	Corr.	4.8−6.4			110	0.050

[a]The best choice of ranges were made such that values of figure of merit, f (see text for definition), achieve minima. For the 6-12 LJ fitting, binding energies, ΔE, and binding lengths, R_e, are also listed.

be unity for CCSD(T)]. For the 6-12 LJ fitting, we chose the estimations achieving minimum f, those with the range R = 4.6−6.4 Å, as finally tabulated in Table 2.

For the correlation fitting, the final choices in Table 2 of main text are also those which achieve minimum f in Table 9, as we did for the 6-12 LJ case. The correlation fitting, if tractable, would be more plausible in the following sense: (i) Its theoretical background is sound (perturbation theory on electron correlation at long-range). (ii) Based on the theory, it is obvious to exclude the repulsive (short-range) region from the fitting region. (iii) Hence there is no ambiguity about the model function to describe the repulsive region such as 6-12/6-9 LJ or 6-exp. (iv) Since ΔE_{corr} increases monotonically, a better and more (numerically) stable fitting can be expected.

APPENDIX E. BINDING LENGTH AND DENSITY

A PES gives a binding length, R_e, which would have some relation to the experimental molecular density. Once some reliable relation is established, we can use it to validate the binding curve calculation. The relation is however not so clear cut, as we describe below. The experimental density of the benzene liquid[89] gives an estimate of mean intermolecular distance as $R_\rho \approx 5.3$ Å, being far larger than R_e in the most stable binding by 26%. This is quite in contrast to the case of A where only the most stable configuration seems dominant. The simplest idea is to take into account the contributions not only from the most stable parallel displacement (ΔE = −2.78 kcal/mol; R_e = 3.87 Å), but also other metastable ones, T-shape (−2.74 kcal/mol; 5.01 Å) and sandwich (−1.81 kcal/mol; 6.09 Å). Only the most unstable configuration (sandwich) has a longer binding length of R = 6.09 Å, and the thermal averaging with the weight $p \approx \exp(-\Delta E/(kT))$ at T = 298.15 K gives $\bar{R}_{dim}$ = 4.5 Å, being 15% underestimation.

As one of the possible origins for the discrepancy, we might consider the intramolecular relaxation, but it is unlikely to account for it: the relaxation will bring energy gains at shorter binding lengths when the molecule deforms by the binding interaction and hence make the binding length shorter, being further away from R_ρ.

Further consideration makes us realize that we took into account only two-body coalescences to argue the mean separation. When we consider further four-body clusterings possibly occurring in realistic liquids, we notice that the mean separation seems to be dominated rather by the longest binding length among the possible coalescence: The mean value can roughly be estimated by an "effective" length of four-body trapezoids, as shown in Figure 5 of main text. Taking the center of gravity of each molecule as the vertices of trapezoids, the "effective lengths" can be defined as the square root of the area of a trapezoid, which is dominated rather by the longest distant binding pair. Estimating the possibility weight for each trapezoid as the Boltzmann weight with the sum of the binding pair energies, ΔE, then the thermal averaging over the "diagonal lengths", l_S = 3.9 Å (sandwich), l_T = 5.1 Å (T-shape), and l_P = 6.0 Å (parallel),[90] gives an improved estimate of $\bar{R}_{tetra}$ = 5.0 Å, getting closer to the experimental estimation of $R_\rho \approx 5.3$ Å.

The discrepancy still left would further be reduced by considering the higher order clustering as well as the atomic vibration at finite temperature,[91] but the present simple idea about four-body trapezoids seems quite successful.

The above scheme also works for CHS, as shown in the main text (See Validation of Equilibrium Properties). For CHS, we can directly estimate the binding energy, ΔE, and the equilibrium binding length, R_e, by fitting the data using an equivalent form of eq 6,

$$U(R) = \Delta E\left[2\left(\frac{R_e}{R}\right)^6 - \left(\frac{R_e}{R}\right)^{12}\right] \quad (9)$$

as summarized in Table 3 of main text. Note that we can also estimate ΔE and R_{eq} "after" the fitting (C_6,C_{12}) first by eq 6 in Appendix D, but this is not a good idea for DMC because the error propagation for statistical noises during the further transformation to ΔE and R_e loses the accuracy of estimates. Fitting curves well describe the dependence around equilibrium lengths, as shown in Figure 2 of main text. For types B and C with shorter-ranged exponents, it is not rigorously validated to use the LJ potential because its functional form assumes the $1/R^6$ asymptotic behavior. We use it, however, under such a

DOI: 10.1021/acs.jctc.6b01159
J. Chem. Theory Comput. 2017, 13, 5217−5230

limited reason just to get possible estimates of ΔE and R_e even for types B and C, as given in Table 1 of main text. Similar to the benzene case, the two-body thermal averaging at T = 298.15 K gives $\bar{R}_{dim} \approx 4.9$ Å, which underestimates $R_\rho \approx 6.8$ Å estimated from experiment. On the other hand, the four-body thermal averaging at the same temperature gives an improved estimate, $\bar{R}_{tetra}$, getting closer to the experimental estimation, as shown in Table 4 of main text.

■ ASSOCIATED CONTENT

Supporting Information

The Supporting Information is available free of charge on the ACS Publications website at DOI: 10.1021/acs.jctc.6b01159.

Additional detail about BSSE and CBS corrections to the SCF and correlated methods and the time-step bias in DMC (PDF)

■ AUTHOR INFORMATION

Corresponding Author

*E-mail: kenta_hongo@mac.com.

ORCID

Kenta Hongo: 0000-0002-2580-0907

Notes

The authors declare no competing financial interest.

■ ACKNOWLEDGMENTS

The authors thank Mr. M. Imamura for his preliminary calculations. K.H. is grateful for financial support from KAKENHI grants (JP15K21023, JP17K17762), a Grant-in-Aid for Scientific Research on Innovative Areas "Mixed Anion" project (JP16H06439) from MEXT, PRESTO (JPMJPR16NA) and the "Materials research by Information Integration Initiative" (MI^2I) project of the Support Program for Starting Up Innovation Hub from Japan Science and Technology Agency (JST). R.M. is grateful to MEXT-KAKENHI (26287063, JP17H05478), the "Mixed Anion" project (JP16H06440), a grant from the Asahi glass Foundation, and US-AFOSR-AOARD for their financial supports. The computation in this work has been mostly done using the facilities of the Research Center for Advanced Computing Infrastructure (RCACI) at JAIST. R.M. and K.H. are also grateful to MEXT-FLAGSHIP2020 (hp170269, hp170220) for their computational resources.

■ REFERENCES

(1) Hamaker, H. The London-van der Waals attractions between sperical particles. *Physica* **1937**, *4*, 1058−1072.

(2) Bonn, D.; Eggers, J.; Indekeu, J.; Meunier, J.; Rolley, E. Wetting and spreading. *Rev. Mod. Phys.* **2009**, *81*, 739−805.

(3) Israelachvili, J. N. *Intermolecular and Surface Forces*, 3rd ed.; Academic Press: San Diego, 2011.

(4) Levy, D., Zayat, M., Eds. *The Sol-Gel Handbook: Synthesis, Characterization and Applications*; Wiley, 2015; 3-volume set.

(5) Shimoda, T.; Matsuki, Y.; Furusawa, M.; Aoki, T.; Yudasaka, I.; Tanaka, H.; Iwasawa, H.; Wang, D.; Miyasaka, M.; Takeuchi, Y. Solution-processed silicon films and transistors. *Nature* **2006**, *440*, 783−786.

(6) Stone, A. J., Ed.*The Theory of Intermolecular Forces*; Oxford University Press: Oxford, U.K., 1997.

(7) Kaplan, I. G., Ed. *Intermolecular Interactions*; J. Wiley & Sons: Chichester, U.K., 2006.

(8) Misquitta, A. J.; Maezono, R.; Drummond, N. D.; Stone, A. J.; Needs, R. J. Anomalous nonadditive dispersion interactions in systems of three one-dimensional wires. *Phys. Rev. B: Condens. Matter Mater. Phys.* **2014**, *89*, 045140.

(9) Tkatchenko, A.; Scheffler, M. Accurate Molecular Van Der Waals Interactions from Ground-State Electron Density and Free-Atom Reference Data. *Phys. Rev. Lett.* **2009**, *102*, 073005.

(10) Lau, P. H.; Takei, K.; Wang, C.; Ju, Y.; Kim, J.; Yu, Z.; Takahashi, T.; Cho, G.; Javey, A. Fully Printed, High Performance Carbon Nanotube Thin-Film Transistors on Flexible Substrates. *Nano Lett.* **2013**, *13*, 3864−3869.

(11) Inoue, S.; Ariga, T.; Matsumoto, S.; Onoue, M.; Miyasako, T.; Tokumitsu, E.; Chinone, N.; Cho, Y.; Shimoda, T. Investigation of solution-processed bismuth-niobium-oxide films. *J. Appl. Phys.* **2014**, *116*, 154103.

(12) Nakamura, Y.; Carlson, A.; Amberg, G.; Shiomi, J. Dynamic wetting at the nanoscale. *Phys. Rev. E* **2013**, *88*, 033010.

(13) Matsui, H.; Noda, Y.; Hasegawa, T. Hybrid Energy-Minimization Simulation of Equilibrium Droplet Shapes on Hydrophilic/Hydrophobic Patterned Surfaces. *Langmuir* **2012**, *28*, 15450−15453.

(14) Cohen, A. J.; Mori-Sánchez, P.; Yang, W. Challenges for Density Functional Theory. *Chem. Rev.* **2012**, *112*, 289−320.

(15) Kim, K. S.; Karthikeyan, S.; Singh, N. J. How Different Are Aromatic π Interactions from Aliphatic π Interactions and Non-π Stacking Interactions? *J. Chem. Theory Comput.* **2011**, *7*, 3471−3477.

(16) Hobza, P.; Muller-Dethlefs, K. *Non-Covalent Interactions*; RSC Theoretical and Computational Chemistry Series; The Royal Society of Chemistry, 2009; pp P001−P226.

(17) Helgaker, T.; Jørgensen, P.; Olsen, P. *Molecular Electronic-Structure Theory*; Wiley: Chichester, U.K., 2000.

(18) Needs, R. J.; Towler, M. D.; Drummond, N. D.; Ríos, P. L. Continuum variational and diffusion quantum Monte Carlo calculations. *J. Phys.: Condens. Matter* **2010**, *22*, 023201.

(19) Austin, B. M.; Zubarev, D. Y.; Lester, W. A. Quantum Monte Carlo and Related Approaches. *Chem. Rev.* **2012**, *112*, 263−288.

(20) Uejima, Y.; Terashima, T.; Maezono, R. Acceleration of a QM/MM-QMC simulation using GPU. *J. Comput. Chem.* **2011**, *32*, 2264−2272.

(21) Uejima, Y.; Maezono, R. GPGPU for orbital function evaluation with a new updating scheme. *J. Comput. Chem.* **2013**, *34*, 83−94.

(22) Hongo, K.; Kawazoe, Y.; Yasuhara, H. Diffusion Monte Carlo Study of Atomic Systems from Li to Ne. *Mater. Trans.* **2006**, *47*, 2612−2616.

(23) Hongo, K.; Kawazoe, Y.; Yasuhara, H. Diffusion Monte Carlo study of correlation in the hydrogen molecule. *Int. J. Quantum Chem.* **2007**, *107*, 1459−1467.

(24) Korth, M.; Luchow, A.; Grimme, S. Toward the Exact Solution of the Electronic Schrodinger Equation for Noncovalent Molecular Interactions: Worldwide Distributed Quantum Monte Carlo Calculations. *J. Phys. Chem. A* **2008**, *112*, 2104−2109.

(25) Horváthová, L.; Dubecký, M.; Mitas, L.; Štich, I. Quantum Monte Carlo Study of π-Bonded Transition Metal Organometallics: Neutral and Cationic VanadiumBenzene and CobaltBenzene Half Sandwiches. *J. Chem. Theory Comput.* **2013**, *9*, 390−400.

(26) Horváthová, L.; Derian, R.; Mitas, L.; Štich, I. Quantum Monte Carlo study of one-dimensional transition-metal organometallic cluster systems and their suitability as spin filters. *Phys. Rev. B: Condens. Matter Mater. Phys.* **2014**, *90*, 115414.

(27) Dubecký, M.; Jurečka, P.; Derian, R.; Hobza, P.; Otyepka, M.; Mitas, L. Quantum Monte Carlo Methods Describe Noncovalent Interactions with Subchemical Accuracy. *J. Chem. Theory Comput.* **2013**, *9*, 4287−4292.

(28) Dubecký, M.; Derian, R.; Jurečka, P.; Mitas, L.; Hobza, P.; Otyepka, M. Quantum Monte Carlo for noncovalent interactions: an efficient protocol attaining benchmark accuracy. *Phys. Chem. Chem. Phys.* **2014**, *16*, 20915−20923.

(29) Hongo, K.; Cuong, N. T.; Maezono, R. The Importance of Electron Correlation on Stacking Interaction of Adenine-Thymine Base-Pair Step in B-DNA: A Quantum Monte Carlo Study. *J. Chem. Theory Comput.* **2013**, *9*, 1081−1086.

(30) Hongo, K.; Watson, M. A.; Sánchez-Carrera, R. S.; Iitaka, T.; Aspuru-Guzik, A. Failure of Conventional Density Functionals for the Prediction of Molecular Crystal Polymorphism: A Quantum Monte Carlo Study. *J. Phys. Chem. Lett.* **2010**, *1*, 1789−1794.
(31) Watson, M. A.; Hongo, K.; Iitaka, T.; Aspuru-Guzik, A. Advances in Quantum Monte Carlo. *ACS Symp. Ser.* **2012**, *1094*, 101−117.
(32) Hongo, K.; Watson, M. A.; Iitaka, T.; Aspuru-Guzik, A.; Maezono, R. Diffusion Monte Carlo Study of Para-Diiodobenzene Polymorphism Revisited. *J. Chem. Theory Comput.* **2015**, *11*, 907−917.
(33) Hongo, K.; Maezono, R. Recent Progress in Quantum Monte Carlo. *ACS Symp. Ser.* **2016**, *1234*, 127−143.
(34) Dubecký, M.; Mitas, L.; Jurečka, P. Noncovalent Interactions by Quantum Monte Carlo. *Chem. Rev.* **2016**, *116*, 5188−5215.
(35) Leong, M. K.; Mastryukov, V. S.; Boggs, J. E. Structure and Conformations of Six-Membered Systems A6H12 (A = C, Si): Ab Initio Study of Cyclohexane and Cyclohexasilane. *J. Phys. Chem.* **1994**, *98*, 6961−6966.
(36) Kormos, B. L.; Cramer, C. J.; Gladfelter, W. L. Pseudo-Two-Dimensional Structures $(HXYH)_{3n}{}^2H_{6n}$ (XY = GaN, SiC, GeC, SiSi, or GeGe; n = 1−3): Density Functional Characterization of Structures and Energetics. *J. Phys. Chem. A* **2006**, *110*, 494−502.
(37) Frisch, M. J.; Trucks, G. W.; Schlegel, H. B.; Scuseria, G. E.; Robb, M. A.; Cheeseman, J. R.; Scalmani, G.; Barone, V.; Mennucci, B.; Petersson, G. A.; Nakatsuji, H.; Caricato, M.; Li, X.; Hratchian, H. P.; Izmaylov, A. F.; Bloino, J.; Zheng, G.; Sonnenberg, J. L.; Hada, M.; Ehara, M.; Toyota, K.; Fukuda, R.; Hasegawa, J.; Ishida, M.; Nakajima, T.; Honda, Y.; Kitao, O.; Nakai, H.; Vreven, T.; Montgomery, J. A., Jr.; Peralta, J. E.; Ogliaro, F.; Bearpark, M.; Heyd, J. J.; Brothers, E.; Kudin, K. N.; Staroverov, V. N.; Kobayashi, R.; Normand, J.; Raghavachari, K.; Rendell, A.; Burant, J. C.; Iyengar, S. S.; Tomasi, J.; Cossi, M.; Rega, N.; Millam, J. M.; Klene, M.; Knox, J. E.; Cross, J. B.; Bakken, V.; Adamo, C.; Jaramillo, J.; Gomperts, R.; Stratmann, R. E.; Yazyev, O.; Austin, A. J.; Cammi, R.; Pomelli, C.; Ochterski, J. W.; Martin, R. L.; Morokuma, K.; Zakrzewski, V. G.; Voth, G. A.; Salvador, P.; Dannenberg, J. J.; Dapprich, S.; Daniels, A. D.; Farkas, O.; Foresman, J. B.; Ortiz, J. V.; Cioslowski, J.; Fox, D. J. *Gaussian 09*, revision D.01; Gaussian, Inc.: Wallingford, CT, 2009.
(38) London, F. The general theory of molecular forces. *Trans. Faraday Soc.* **1937**, *33*, 8b−26.
(39) Grimme, S.; Hansen, A.; Brandenburg, J. G.; Bannwarth, C. Dispersion-Corrected Mean-Field Electronic Structure Methods. *Chem. Rev.* **2016**, *116*, 5105−5154.
(40) Choi, S.-B.; Kim, B.-K.; Boudjouk, P.; Grier, D. G. Amine-Promoted Disproportionation and Redistribution of Trichlorosilane: Formation of Tetradecachlorocyclohexasilane Dianion. *J. Am. Chem. Soc.* **2001**, *123*, 8117−8118.
(41) Kumar, A.; Meath, W. J. Dipole oscillator strength properties and dispersion energies for acetylene and benzene. *Mol. Phys.* **1992**, *75*, 311−324.
(42) Jiemchooroj, A.; Norman, P.; Sernelius, B. E. Complex polarization propagator method for calculation of dispersion coefficients of extended π-conjugated systems: The C6 coefficients of polyacenes and C60. *J. Chem. Phys.* **2005**, *123*, 124312.
(43) Marques, M. A. L.; Castro, A.; Malloci, G.; Mulas, G.; Botti, S. Efficient calculation of van der Waals dispersion coefficients with time-dependent density functional theory in real time: Application to polycyclic aromatic hydrocarbons. *J. Chem. Phys.* **2007**, *127*, 014107.
(44) Lifshitz, E. The theory of molecular attractive forces between solids. *Soviet Phys. JETP* **1956**, *2*, 73−83.
(45) Botti, S.; Castro, A.; et al. Cluster-surface and cluster-cluster interactions: Ab initio calculations and modeling of asymptotic van der Waals forces. *Phys. Rev. B: Condens. Matter Mater. Phys.* **2008**, *78*, 035333.
(46) Greenwood, N. N.; Earnshaw, A. *Chemistry of the Elements*, 2nd ed.; Butterworth-Heinemann, 1997.
(47) Boys, S.; Bernardi, F. The calculation of small molecular interactions by the differences of separate total energies. Some procedures with reduced errors. *Mol. Phys.* **1970**, *19*, 553−566.
(48) van Duijneveldt, F. B.; van Duijneveldt-van de Rijdt, J. G. C. M.; van Lenthe, J. H. State of the Art in Counterpoise Theory. *Chem. Rev.* **1994**, *94*, 1873−1885.
(49) Simon, S.; Duran, M.; Dannenberg, J. J. How does basis set superposition error change the potential surfaces for hydrogen-bonded dimers? *J. Chem. Phys.* **1996**, *105*, 11024−11031.
(50) Tkatchenko, A.; von Lilienfeld, O. A. Popular Kohn-Sham density functionals strongly overestimate many-body interactions in van der Waals systems. *Phys. Rev. B: Condens. Matter Mater. Phys.* **2008**, *78*, 045116.
(51) Grimme, S. Semiempirical GGA-type density functional constructed with a long-range dispersion correction. *J. Comput. Chem.* **2006**, *27*, 1787−1799.
(52) Grimme, S.; Antony, J.; Ehrlich, S.; Krieg, H. A consistent and accurate ab initio parametrization of density functional dispersion correction (DFT-D) for the 94 elements H-Pu. *J. Chem. Phys.* **2010**, *132*, 154104.
(53) Riley, K. E.; Platts, J. A.; Řezáč, J.; Hobza, P.; Hill, J. G. Assessment of the Performance of MP2 and MP2 Variants for the Treatment of Noncovalent Interactions. *J. Phys. Chem. A* **2012**, *116*, 4159−4169.
(54) Sinnokrot, M. O.; Sherrill, C. D. Highly Accurate Coupled Cluster Potential Energy Curves for the Benzene Dimer: Sandwich, T-Shaped, and Parallel-Displaced Configurations. *J. Phys. Chem. A* **2004**, *108*, 10200−10207.
(55) Reynolds, P. J.; Ceperley, D. M.; Alder, B. J.; Lester, W. A. Fixed-node quantum Monte Carlo for molecules. *J. Chem. Phys.* **1982**, *77*, 5593−5603.
(56) Mitáš, L.; Shirley, E. L.; Ceperley, D. M. Nonlocal pseudopotentials and diffusion Monte Carlo. *J. Chem. Phys.* **1991**, *95*, 3467−3475.
(57) Casula, M. Beyond the locality approximation in the standard diffusion Monte Carlo method. *Phys. Rev. B: Condens. Matter Mater. Phys.* **2006**, *74*, 161102.
(58) Hongo, K.; Maezono, R. A benchmark quantum Monte Carlo study of the ground state chromium dimer. *Int. J. Quantum Chem.* **2012**, *112*, 1243−1255.
(59) Kolorenč, J.; Hu, S.; Mitas, L. Wave functions for quantum Monte Carlo calculations in solids: Orbitals from density functional theory with hybrid exchange-correlation functionals. *Phys. Rev. B: Condens. Matter Mater. Phys.* **2010**, *82*, 115108.
(60) Per, M. C.; Walker, K. A.; Russo, S. P. How Important is Orbital Choice in Single-Determinant Diffusion Quantum Monte Carlo Calculations? *J. Chem. Theory Comput.* **2012**, *8*, 2255−2259.
(61) Hongo, K.; Maezono, R. Advances in Quantum Monte Carlo. *ACS Symp. Ser.* **2012**, *1094*, 91−99.
(62) Masuda, T.; Matsuki, Y.; Shimoda, T. Spectral parameters and Hamaker constants of silicon hydride compounds and organic solvents. *J. Colloid Interface Sci.* **2009**, *340*, 298−305.
(63) Řezáč, J.; Hobza, P. Describing Noncovalent Interactions beyond the Common Approximations: How Accurate Is the "Gold Standard," CCSD(T) at the Complete Basis Set Limit? *J. Chem. Theory Comput.* **2013**, *9*, 2151−2155.
(64) Truhlar, D. G. Basis-set extrapolation. *Chem. Phys. Lett.* **1998**, *294*, 45−48.
(65) Maezono, R. Optimization of Many-Body Wave Function. *J. Comput. Theor. Nanosci.* **2009**, *6*, 2474−2482.
(66) Harding, M. E.; Metzroth, T.; Gauss, J.; Auer, A. A. Parallel Calculation of CCSD and CCSD(T) Analytic First and Second Derivatives. *J. Chem. Theory Comput.* **2008**, *4*, 64−74.
(67) Burkatzki, M.; Filippi, C.; Dolg, M. Energy-consistent pseudopotentials for quantum Monte Carlo calculations. *J. Chem. Phys.* **2007**, *126*, 234105.
(68) Jastrow, R. Many-Body Problem with Strong Forces. *Phys. Rev.* **1955**, *98*, 1479−1484.
(69) Drummond, N. D.; Towler, M. D.; Needs, R. J. Jastrow correlation factor for atoms, molecules, and solids. *Phys. Rev. B: Condens. Matter Mater. Phys.* **2004**, *70*, 235119.

DOI: 10.1021/acs.jctc.6b01159
J. Chem. Theory Comput. 2017, 13, 5217−5230

(70) Umrigar, C. J.; Filippi, C. Energy and Variance Optimization of Many-Body Wave Functions. *Phys. Rev. Lett.* **2005**, *94*, 150201.
(71) Drummond, N. D.; Needs, R. J. Variance-minimization scheme for optimizing Jastrow factors. *Phys. Rev. B: Condens. Matter Mater. Phys.* **2005**, *72*, 085124.
(72) Kato, T. On the eigenfunctions of many-particle systems in quantum mechanics. *Comm. Pure Appl. Math.* **1957**, *10*, 151−177.
(73) Umrigar, C. J.; Nightingale, M. P.; Runge, K. J. A diffusion Monte Carlo algorithm with very small time-step errors. *J. Chem. Phys.* **1993**, *99*, 2865−2890.
(74) Zhao, Y.; Truhlar, D. The M06 suite of density functionals for main group thermochemistry, thermochemical kinetics, noncovalent interactions, excited states, and transition elements: two new functionals and systematic testing of four M06-class functionals and 12 other functionals. *Theor. Chem. Acc.* **2008**, *120*, 215−241.
(75) Vosko, S. H.; Wilk, L.; Nusair, M. Accurate spin-dependent electron liquid correlation energies for local spin density calculations: a critical analysis. *Can. J. Phys.* **1980**, *58*, 1200−1211.
(76) Perdew, J. P.; Burke, K.; Ernzerhof, M. Generalized Gradient Approximation Made Simple. *Phys. Rev. Lett.* **1996**, *77*, 3865−3868.
(77) Lee, C.; Yang, W.; Parr, R. G. Development of the Colle-Salvetti correlation-energy formula into a functional of the electron density. *Phys. Rev. B: Condens. Matter Mater. Phys.* **1988**, *37*, 785−789.
(78) Becke, A. D. Density-functional thermochemistry. III. The role of exact exchange. *J. Chem. Phys.* **1993**, *98*, 5648−5652.
(79) Stephens, P. J.; Devlin, F. J.; Chabalowski, C. F.; Frisch, M. J. Ab Initio Calculation of Vibrational Absorption and Circular Dichroism Spectra Using Density Functional Force Fields. *J. Phys. Chem.* **1994**, *98*, 11623−11627.
(80) Casimir, H. B. G.; Polder, D. The Influence of Retardation on the London-van der Waals Forces. *Phys. Rev.* **1948**, *73*, 360−372.
(81) Podeszwa, R.; Bukowski, R.; Szalewicz, K. Potential Energy Surface for the Benzene Dimer and Perturbational Analysis of π-π Interactions. *J. Phys. Chem. A* **2006**, *110*, 10345−10354.
(82) Parsegian, V.; Ninham, B. Application of the Lifshitz Theory to the Calculation of Van der Waals Forces across Thin Lipid Films. *Nature* **1969**, *224*, 1197.
(83) Ninham, B.; Parsegian, V. van der Waals Forces. *Biophys. J.* **1970**, *10*, 646−663.
(84) Zeinalipour-Yazdi, C. D.; Pullman, D. P. Correlation of Polarizabilities with Van Der Waals Interactions in π-systems. *J. Phys. Chem. B* **2006**, *110*, 24260−24265.
(85) Azadi, S.; Cohen, R. E. Chemical accuracy from quantum Monte Carlo for the benzene dimer. *J. Chem. Phys.* **2015**, *143*, 104301.
(86) Park, Y. C.; Lee, J. S. Accurate ab Initio Binding Energies of the Benzene Dimer. *J. Phys. Chem. A* **2006**, *110*, 5091−5095.
(87) Buckingham, R. A. The Classical Equation of State of Gaseous Helium, Neon and Argon. *Proc. R. Soc. London, Ser. A* **1938**, *168*, 264−283.
(88) Hobza, P.; Selzle, H. L.; Schlag, E. W. Potential Energy Surface for the Benzene Dimer. Results of ab Initio CCSD(T) Calculations Show Two Nearly Isoenergetic Structures: T-Shaped and Parallel-Displaced. *J. Phys. Chem.* **1996**, *100*, 18790−18794.
(89) Haynes, W. M., Ed. *CRC Handbook of Chemistry and Physics*, 94th ed.; CRC Press LLC, 2013; pp 3−34.
(90) Bludský, O.; Rubeš, M.; Soldán, P.; Nachtigall, P. Investigation of the benzene-dimer potential energy surface: DFT/CCSD(T) correction scheme. *J. Chem. Phys.* **2008**, *128*, 114102.
(91) Nakano, K.; Hongo, K.; Maezono, R. Phonon dispersions and Fermi surfaces nesting explaining the variety of charge ordering in titanium-oxypnictides superconductors. *Sci. Rep.* **2016**, *6*, 29661.

DOI: 10.1021/acs.jctc.6b01159
J. Chem. Theory Comput. 2017, 13, 5217−5230